Fermi-surface structure of potassium in the charge-density-wave state

Yong Gyoo Hwang and A. W. Overhauser
Department of Physics, Purdue University, West Lafayette, Indiana 47907
(Received 8 March 1988)

The neutron-diffraction determination of the charge-density-wave (CDW) wave vector $\mathbf{Q}$ in potassium is used to calculate the detailed structure of the conduction-electron Fermi surface. A Schrödinger equation having two periodic potentials, $2\alpha\cos(\mathbf{Q}\cdot\mathbf{r})$ from the CDW, and $2\beta\cos(\mathbf{G}\cdot\mathbf{r})$ from the lattice, is solved numerically. Minigaps in $E(\mathbf{k})$, caused by perturbations having periodicity $(n+1)\mathbf{Q}-n\mathbf{G}$, $n=1,2,\ldots$, lead to small cylindrical sections of Fermi surface. These cylinders give rise to perpendicular-field cyclotron resonance and unexpected angle-resolved photoemission peaks. Heterodyne gaps, having periodicity $n(\mathbf{G}-\mathbf{Q})$, are created in the equatorial region of the Fermi "sphere." Open-orbit magnetoresistance peaks observed by Coulter and Datars (in K and Na) arise from the multiply connected Fermi-surface topology caused by the minigaps and heterodyne gaps.

I. INTRODUCTION

It has long been held that the energy spectrum $E(\mathbf{k})$ of conduction electrons in alkali metals is nearly parabolic, and that the Fermi surface is nearly spherical (and consequently simply connected). However, there has been a large accumulation of experimental data[1] which suggest a nonspherical and multiply connected structure for the Fermi surface. The microscopic theory of charge-density-wave (CDW) instability[2] explains the existence of such Fermi-surface structure and provides successful explanations of most of the anomalous data.[1]

In a CDW state, a sinusoidal modulation of electronic charge density is sustained self-consistently through exchange and correlation interactions, and gives rise to a sinusoidal potential incommensurate with the usual crystal potential. As a result, the Fermi surface suffers a distortion, and is sliced into many pieces by extra energy gaps. The modulated electron charge density is neutralized by a sinusoidal deformation of the positive-ion background. This lattice deformation contributes extra diffraction peaks in a neutron-scattering experiment. These satellite reflections have been observed by Giebultowicz *et al.*[3] (GOW), and the CDW wave vector $\mathbf{Q}$ was determined accurately.

Subsequent work by Pintschovius *et al.*[4] (PB) has suggested that the satellites observed by GOW were instead experimental artifacts caused by double scattering.[5] However, recent experiments[6] by Werner *et al.* (WOG) have shown that the satellites observed by GOW have the *same* spacing near the (220) Bragg point as they have near the (110) point. Double-scattering artifacts exhibit spacings proportional to $\tan\theta_B$, where θ_B is the Bragg angle, and would have to be 2.5 times further off the [110] axis near the (220) Bragg point compared to their spacing near the (110) point. The samples used by PB showed an incremental increase in mosaic width on each cooldown.[4] Consequently they were severely plastically deformed, and neutron scattering from dislocations exceeded by 2 orders of magnitude the total incoherent scattering observed by GOW and WOG in their stress-free sample. Consequently PB could not have observed CDW satellites. The structure PB reported was indeed caused by double scattering originating from the severe plastic strain.

The purpose of this study is to calculate the detailed structure of the Fermi surface of potassium based on the neutron-diffraction measurement of the CDW wave vector $\mathbf{Q}$. In Sec. II, effects of the CDW potential will be discussed. In Sec. III, the approximate shape of the Fermi surface is found. The results are summarized in Sec. IV.

II. PLANE-WAVE EXPANSION

To find the energy spectrum for conduction electrons in a CDW state, one has to solve a Schrödinger equation with two sinusoidal potentials, one arising from the crystal structure and the other from the CDW instability:

$$\left[-\frac{\hbar^2}{2m}\nabla^2+V(\mathbf{r})\right]\Psi=E\Psi\ , \tag{1}$$

where

$$\mathbf{V}(r)=2\alpha\cos(\mathbf{Q}\cdot\mathbf{r})+2\beta\cos(\mathbf{G}\cdot\mathbf{r})\ . \tag{2}$$

$\mathbf{Q}$ is the CDW wave vector, $\mathbf{Q}=(0.995,0.975,0.015)$,[3] and $\mathbf{G}$ is the $\langle 110\rangle$ reciprocal-lattice vector, with $\mathbf{G}=(1,1,0)$ in units of $2\pi/a$, where a is the lattice constant of the bcc lattice. 2α is the CDW potential and is about 0.87 eV (the CDW energy gap is about 0.62 eV), as indicated by the threshold of the Mayer–El Naby optical anomaly.[7] 2β is the Brillouin-zone energy gap and is approximately 0.40 eV, as derived from an analysis of de Haas–van Alphen data.[8] We will neglect contributions of the other five pseudopotentials, oriented 60° or 90° away from $\mathbf{G}_{110}$, since the coupling through them involves plane-wave states with energies too far removed to contribute significantly.

We choose a coordinate system such that $\mathbf{G}=G\hat{\mathbf{z}}$ and $\hat{\mathbf{y}}$ is parallel to $\mathbf{G}\times\mathbf{Q}$,

 ©1989 The American Physical Society

$$\mathbf{Q}=(Q_x,0,Q_z)\ , \tag{3a}$$

$$\mathbf{G}=(0,0,G)\ . \tag{3b}$$

The angle between $\mathbf{Q}$ and $\mathbf{G}$ is 0.85°, and $Q/G\cong 0.985$. When $\mathbf{Q}$ is parallel to $\mathbf{G}$, the potential $V(\mathbf{r})$ does not have a translational symmetry. An approximate energy spectrum was obtained for this case by Fragachan and Overhauser.[9]

The potential $V(\mathbf{r})$ in Eq. (2) is periodic under a translation through the vector $\mathbf{R}$,

$$\mathbf{R}=m\mathbf{a}_1+n\mathbf{a}_2\ , \tag{4}$$

where

$$\mathbf{a}_1=(-Q_z/Q_x,0,1)\cong(-67.6,0,1)\ , \tag{5a}$$

$$\mathbf{a}_2=((G-Q_z)/Q_x,0,1)\cong(1.03,0,1)\ . \tag{5b}$$

The size of this unit cell is 68.6 times that of the primitive bcc unit cell. The corresponding reciprocal-lattice vectors are

$$\mathbf{b}_1=\mathbf{G}-\mathbf{Q}=\mathbf{Q}'\ , \tag{6a}$$

$$\mathbf{b}_2=\mathbf{Q}\ . \tag{6b}$$

The angle between $\mathbf{Q}'$ and $\mathbf{G}$ is 44.2°, and $Q'/G=0.021$. The size of the new Brillouin zone is about 0.014 times that of the bcc Brillouin zone. As a result, the reciprocal-space structure is much more complicated, especially near the Fermi surface.

According to Bloch's theorem, wave functions have the following form:

$$\Psi_{\mathbf{k}}=e^{i\mathbf{k}\cdot\mathbf{r}}u_{\mathbf{k}}(\mathbf{r})\ , \tag{7}$$

where $u_{\mathbf{k}}(\mathbf{r}+\mathbf{R})=u_{\mathbf{k}}(\mathbf{r})$ and $\mathbf{k}$ is quantized in accord with the periodic boundary conditions,

$$\Psi(N_1\mathbf{a}_1+\mathbf{r})=\Psi(\mathbf{r})\ , \tag{8a}$$

$$\Psi(N_2\mathbf{a}_2+\mathbf{r})=\Psi(\mathbf{r})\ . \tag{8b}$$

N_1a_1 and N_2a_2 are the sizes of the sample in the directions $\mathbf{a}_1$ and $\mathbf{a}_2$, respectively. $u_{\mathbf{k}}(\mathbf{r})$ can be expanded in terms of plane-wave states,

$$u_{\mathbf{k}}(\mathbf{r})=\sum_{m',n'}a_{m'n'}e^{i(m'\mathbf{b}_1+n'\mathbf{b}_2)\cdot\mathbf{r}}=\sum_{m,n}a_{mn}e^{i(m\mathbf{Q}+n\mathbf{G})\cdot\mathbf{r}}\ . \tag{9}$$

The Schrödinger equation can be put into matrix form:

$$\sum_{m',n'}\left\{\frac{\hbar^2}{2m}(\mathbf{k}+m\mathbf{Q}+n\mathbf{G})^2\delta_{m,m'}\delta_{n,n'}+\alpha(\delta_{m,m'-1}+\delta_{m,m'+1})\delta_{n,n'}+\beta\delta_{m,m'}(\delta_{n,n'-1}+\delta_{n,n'+1})\right\}a_{m'n'}=E(\mathbf{k})a_{mn}\ . \tag{10}$$

By solving these matrix equations, one finds the energy spectrum and the wave functions. Each state $|\mathbf{k}\rangle$ is coupled to $|\mathbf{k}\pm\mathbf{Q}\rangle$ through the CDW potential and to $|\mathbf{k}\pm\mathbf{G}\rangle$ through the crystal potential. Since the matrix Schrödinger equation cannot be solved exactly, we resort to an approximate scheme presented in the next section.

III. APPROXIMATE SOLUTIONS

Since the potential given by Eq. (2) does not have any geometrical symmetry other than inversion, the zone structure determined by energy gaps, which in general are curved surfaces, need not be the same as the Brillouin zone structure. But they should not be drastically different because the energy-gap surfaces pass through the points $(m\mathbf{Q}+n\mathbf{G})/2$. The zone structure determined by energy gaps can be shown to be equivalent to the Brillouin-zone structure obtained from cutting and rearranging zones determined by planes bisecting reciprocal-lattice vectors.[10]

To find the Fermi surface, we consider a constant energy surface in the extended-Brillouin-zone scheme. Near the Fermi surface, two distinct groups of zone boundaries are important: (a) minigap zone boundaries passing through $\mathbf{K}_n/2=[(n+1)\mathbf{Q}-n\mathbf{G}]/2$, where $n=0,1,2,\ldots$, and (b) heterodyne-gap zone boundaries passing through $\mathbf{H}_n/2=n(\mathbf{G}-\mathbf{Q})/2$, where $n=1,2,\ldots$. Since the Fermi surface has inversion symmetry, we will consider only $\mathbf{k}\cdot\hat{\mathbf{Q}}\geq 0$.

A. Near $\mathbf{k}\cdot\hat{\mathbf{Q}}\cong Q/2$ (minigap region)

Because of the small differences in magnitude and direction of $\mathbf{G}$ and $\mathbf{Q}$, heterodyne gaps near $\mathbf{Q}/2$ are of very high order. These gaps can be neglected since the size of an energy gap decreases very rapidly as the order of gap increases, as can be seen in Table I. The sizes of the minigaps in Table I were calculated parallel to $\hat{\mathbf{Q}}$ starting from $\mathbf{Q}/2$ using the approximation explained in Sec. III B.

Approximate solutions of the matrix Schrödinger equation can be found by neglecting couplings between states too far apart in energy. There are two distinct series of minigaps. The minimum number of states needed to calculate the energy spectrum in this region are as follows.

(i) Even-integer minigaps involving states separated by $\mathbf{K}_{2m}=(2m+1)\mathbf{Q}-2m\mathbf{G}$, where $m=0,1,2,\ldots$.

TABLE I. Sizes of CDW energy gaps.

Order of gap	Heterodyne gap (meV)	Minigap (meV)
1	16	90
2	14	67
3	12	51
4	8	34
5	3	15
6	0.6	4
7	0.06	0.6
8	0.01	0.06

The zeroth minigap (CDW main gap):

$|\mathbf{k}\rangle$, $|\mathbf{k}-\mathbf{Q}\rangle$.

The second minigap: the above set and

$|\mathbf{k}-\mathbf{Q}+\mathbf{G}\rangle$, $|\mathbf{k}-2\mathbf{Q}+\mathbf{G}\rangle$,

$|\mathbf{k}-2\mathbf{Q}+2\mathbf{G}\rangle$, $|\mathbf{k}-3\mathbf{Q}+2\mathbf{G}\rangle$.

The fourth minigap: the above sets and

$|\mathbf{k}-3\mathbf{Q}+3\mathbf{G}\rangle$, $|\mathbf{k}-4\mathbf{Q}+3\mathbf{G}\rangle$,

$|\mathbf{k}-4\mathbf{Q}+4\mathbf{G}\rangle$, $|\mathbf{k}-5\mathbf{Q}+4\mathbf{G}\rangle$,

etc.

(ii) Odd-integer minigaps involving states separated by $\mathbf{K}_{2m+1}=(2m+2)\mathbf{Q}-(2m+1)\mathbf{G}$, where $m=0,1,2,\ldots$.

The first minigap:

$|\mathbf{k}\rangle$, $|\mathbf{k}-\mathbf{Q}\rangle$, $|\mathbf{k}-\mathbf{Q}+\mathbf{G}\rangle$, $|\mathbf{k}-2\mathbf{Q}+\mathbf{G}\rangle$.

The third minigap: the above set and

$|\mathbf{k}-2\mathbf{Q}+2\mathbf{G}\rangle$, $|\mathbf{k}-3\mathbf{Q}+2\mathbf{G}\rangle$,

$|\mathbf{k}-3\mathbf{Q}+3\mathbf{G}\rangle$, $|\mathbf{k}-4\mathbf{Q}+3\mathbf{G}\rangle$.

The fifth minigap: the above sets and

$|\mathbf{k}-4\mathbf{Q}+4\mathbf{G}\rangle$, $|\mathbf{k}-5\mathbf{Q}+4\mathbf{G}\rangle$,

$|\mathbf{k}-5\mathbf{Q}+5\mathbf{G}\rangle$, $|\mathbf{k}-6\mathbf{Q}+5\mathbf{G}\rangle$,

etc.

Equal numbers of states above and below (in energy) compared to the states required in the minimum sets were included. Dimensions of matrices diagonalized were 30×30 near even-integer minigap surfaces and 28×28 near odd-integer minigap surfaces. The cross section of the Fermi surface in the $\hat{\mathbf{G}}$-$\hat{\mathbf{Q}}$ plane is shown in Fig. 1. The energy spectrum is approximately cylindrical. Note the small cylindrical sections near $\mathbf{Q}/2$, which cause the perpendicular-field cyclotron resonance[11] as well as unexpected sharp peaks in recent angle-resolved photoemission data.[12]

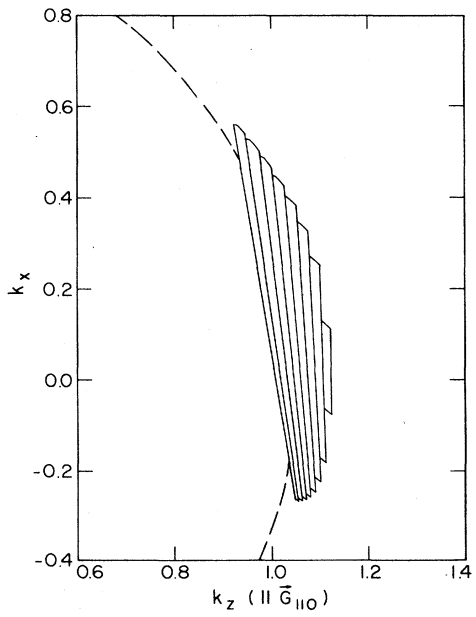

FIG. 1. Approximate shape of the Fermi surface in the minigap region ($\mathbf{k}\cdot\hat{\mathbf{Q}}\cong Q/2$) for $E(\mathbf{k})=2.35$ eV. k_z and k_x are in units of k_F. The dashed curve is that of a free-electron Fermi sphere having the same energy.

B. Near $\mathbf{k}\cdot\hat{\mathbf{Q}}'\cong Q'$ (heterodyne-gap region)

Near this equatorial region minigaps are of very high order and can be neglected, since the size of an energy gap decreases very rapidly as the order of the gap increases, as can be seen in Table I. The sizes of the heterodyne gaps in Table I were calculated parallel to $\hat{\mathbf{Q}}'$, starting from the origin and with use of the approximation explained in Sec. III A.

Approximate solutions can be found by neglecting couplings between states too far apart in energy. There are two distinct series of heterodyne gaps. The minimum number of states needed to calculate the energy spectrum in this region are as follows.

(i) Odd-integer heterodyne gaps involving states separated by $\mathbf{H}_{2m-1}=(2m-1)\mathbf{Q}'$, where $m=1,2,\ldots$.

The first heterodyne gap:

$|\mathbf{k}\rangle$, $|\mathbf{k}+\mathbf{Q}\rangle$, $|\mathbf{k}+\mathbf{Q}-\mathbf{G}\rangle$, $|\mathbf{k}-\mathbf{G}\rangle$.

The third heterodyne gap: the above set and

$|\mathbf{k}+2\mathbf{Q}-\mathbf{G}\rangle$, $|\mathbf{k}+2\mathbf{Q}-2\mathbf{G}\rangle$, $|\mathbf{k}+\mathbf{Q}-2\mathbf{G}\rangle$,

$|\mathbf{k}+3\mathbf{Q}-2\mathbf{G}\rangle$, $|\mathbf{k}+3\mathbf{Q}-3\mathbf{G}\rangle$, $|\mathbf{k}+2\mathbf{Q}-3\mathbf{G}\rangle$.

The fifth heterodyne gap: the above sets and

$|\mathbf{k}+4\mathbf{Q}-3\mathbf{G}\rangle$, $|\mathbf{k}+4\mathbf{Q}-4\mathbf{G}\rangle$, $|\mathbf{k}+3\mathbf{Q}-4\mathbf{G}\rangle$,

$|\mathbf{k}+5\mathbf{Q}-4\mathbf{G}\rangle$, $|\mathbf{k}+5\mathbf{Q}-5\mathbf{G}\rangle$, $|\mathbf{k}+4\mathbf{Q}-5\mathbf{G}\rangle$,

etc.

(ii) Even-integer heterodyne gaps involving states separated by $\mathbf{H}_{2m}=2m\mathbf{Q}'$, where $m=1,2,\ldots$.

The second heterodyne gap:

$|\mathbf{k}\rangle$, $|\mathbf{k}+\mathbf{Q}\rangle$, $|\mathbf{k}+\mathbf{Q}-\mathbf{G}\rangle$, $|\mathbf{k}-\mathbf{G}\rangle$,

$|\mathbf{k}+2\mathbf{Q}-\mathbf{G}\rangle$, $|\mathbf{k}+2\mathbf{Q}-2\mathbf{G}\rangle$, $|\mathbf{k}+\mathbf{Q}-2\mathbf{G}\rangle$.

The fourth heterodyne gap: the above set and

$|\mathbf{k}+3\mathbf{Q}-2\mathbf{G}\rangle$, $|\mathbf{k}+3\mathbf{Q}-3\mathbf{G}\rangle$, $|\mathbf{k}+2\mathbf{Q}-3\mathbf{G}\rangle$,

$|\mathbf{k}+4\mathbf{Q}-3\mathbf{G}\rangle$, $|\mathbf{k}+4\mathbf{Q}-4\mathbf{G}\rangle$, $|\mathbf{k}+3\mathbf{Q}-4\mathbf{G}\rangle$.

The sixth heterodyne gap: the above sets and

$|\mathbf{k}-5\mathbf{Q}-4\mathbf{G}\rangle$, $|\mathbf{k}-5\mathbf{Q}-5\mathbf{G}\rangle$, $|\mathbf{k}+4\mathbf{Q}-5\mathbf{G}\rangle$,

$|\mathbf{k}+6\mathbf{Q}-5\mathbf{G}\rangle$, $|\mathbf{k}+6\mathbf{Q}-6\mathbf{G}\rangle$, $|\mathbf{k}+5\mathbf{Q}-6\mathbf{G}\rangle$,

etc.

Equal numbers of states above and below (in energy) compared to the states required in the minimum sets were included as before. Dimensions of matrices diagonalized were 31×31 near even-integer heterodyne-gap

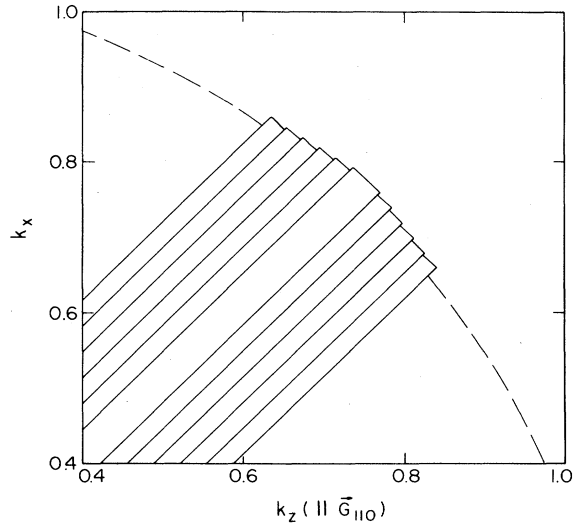

FIG. 2. Approximate shape of the Fermi surface in the heterodyne gap region ($\mathbf{k}\cdot\hat{\mathbf{Q}}' \cong Q'/2$) for $E(\mathbf{k})=2.35$ eV. k_z and k_x are in units of k_F. The dashed curve is that of a free-electron Fermi sphere having the same energy.

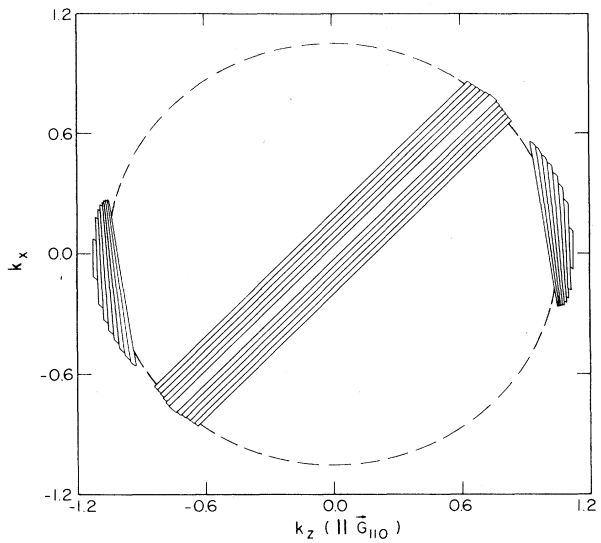

FIG. 3. Approximate shape of the Fermi surface for $E(\mathbf{k})=2.35$ eV. k_z and k_x are in units of k_F. The dashed curve is that of a free-electron Fermi sphere having the same energy.

surfaces and 28×28 near odd-integer heterodyne-gap surfaces. The cross section of the Fermi surface in the $\hat{\mathbf{G}}$-$\hat{\mathbf{Q}}$ plane is shown in Fig. 2. The energy spectrum is approximately symmetric about $\hat{\mathbf{Q}}'$ in this region. Note the truncations of the Fermi surface, which lead to the presence of open orbits. Open-orbit motion is responsible for magnetoresistance peaks[13] and splittings of the spin-wave sidebands in conduction-electron spin-resonance transmission experiments.[14]

IV. CONCLUSIONS

The Fermi surface of potassium is shown to be anisotropic and multiply connected by solving a Schrödinger equation having two sinusoidal potentials: one from the CDW and the other from the lattice. An approximate shape of the Fermi surface, calculated numerically, is shown in Fig. 3. The Fermi energy was chosen to be 2.35 eV so that the radius of the smallest cylindrical section is about $0.1k_F$, a value required to explain the perpendicular-field cyclotron resonance.[11] (The diameters of the cylindrical sections near the main gap depend on the Fermi energy and their positions relative to the CDW gap, which are not known.) Far off the $\hat{\mathbf{G}}$-$\hat{\mathbf{Q}}$ plane, the contributions of other pseudopotentials may not be neglected and the actual Fermi surface may be different from that suggested in Fig. 3. The Fermi surface is sliced into many pieces by two families of extra energy gaps: minigaps and heterodyne gaps. Minigaps are caused by perturbations having periodicity $\mathbf{K}_n=(n+1)\mathbf{Q}-n\mathbf{G}$, where $n=0,1,2,\ldots$. The presence of cylindrical sections near $|\mathbf{k}|\cong Q/2$ is responsible for the perpendicular-field cyclotron resonance. Heterodyne gaps are caused by perturbations with periodicity $\mathbf{H}_n=n(\mathbf{G}-\mathbf{Q})$, where $n=1,2,\ldots$. The occurrence of open orbits caused by these extra energy gaps leads to the open-orbit magnetoresistance peaks observed by Coulter and Datars.[13] CDW-domain patterns (arising from the 24 crystallographically equivalent directions of $\mathbf{Q}$) play an important role in explaining the observed splitting of the conduction-electron spin resonance[15] and that of the spin-wave sidebands in transmission experiments.[14]

We emphasize as a final remark that the data in Table I, and the details of the Fermi surface shown in Fig. 3 are merely suggestive. Since the exchange and correlation potentials which cause a CDW are highly nonlocal,[16,17] the CDW potential 2α will be a (possibly rapid) function of $\mathbf{k}$. Such nonlocal effects have been ignored in the exercise presented here. They were estimated in a calculation of the fractional charge modulation of the CDW;[18] and the result was a 40% reduction in the predicted CDW charge modulation. We anticipate that if the $\mathbf{k}$ dependence of 2α were included in the calculations presented here, then the minigaps and heterodyne gaps would fall off more rapidly with increasing order than the sequence shown in Table I.

ACKNOWLEDGMENTS

This work was supported by the Materials Research Laboratory Program of the National Science Foundation.

[1]A. W. Overhauser, in *Highlights of Condensed-Matter Theory*, Proceedings of the International School of Physics "Enrico Fermi," Course LXXXIX, edited by F. Bassani, F. Fumi, and M. P. Tosi (North-Holland, Amsterdam, 1985); A. W. Overhauser, Adv. Phys. **27**, 343 (1978).

[2]A. W. Overhauser, Phys. Rev. **128**, 1437 (1962); **167**, 691 (1968).

[3]T. M. Giebultowicz, A. W. Overhauser, and S. A. Werner,

Phys. Rev. Lett. **56**, 1485 (1986); S. A. Werner, T. M. Giebultowicz, and A. W. Overhauser, Phys. Scr. **T19**, 266 (1987).
[4]L. Pintschovius, O. Blaschko, G. Krexner, M. de Podesta, and R. Currat, Phys. Rev. B **35**, 9330 (1987); O. Blaschko, M. de Podesta, and L. Pintschovius, *ibid.* **37**, 4258 (1988).
[5]T. M. Giebultowicz, A. W. Overhauser, and S. A. Werner, Phys. Rev. Lett. **56**, 2228 (1986); S. A. Werner and M. Arif, Acta Crystallogr. Sect. A **44**, 383 (1988).
[6]S. A. Werner, A. W. Overhauser, and T. M. Giebultowicz (unpublished).
[7]H. Mayer and M. H. El Naby, Z. Phys. **174**, 269 (1963); A. W. Overhauser, Phys. Rev. Lett. **13**, 190 (1964).
[8]N. Ashcroft, Phys. Rev. **140**, A935 (1965).
[9]F. E. Fragachan and A. W. Overhauser, Phys. Rev. B **29**, 2912 (1984).
[10]F. Seitz, *The Modern Theory of Solids* (McGraw-Hill, New York, 1940), Sec. 61.
[11]G. Lacueva and A. W. Overhauser, Phys. Rev. B **33**, 3765 (1986).
[12]E. Jensen and E. W. Plummer, Phys. Rev. Lett. **55**, 1912 (1985); A. W. Overhauser, *ibid.* **55**, 1916 (1985).
[13]P. G. Coulter and W. R. Datars, Phys. Rev. Lett. **45**, 1021 (1980); Solid State Commun. **43**, 715 (1982); Can. J. Phys. **63**, 159 (1985).
[14]Y. G. Hwang and A. W. Overhauser, Phys. Rev. B **38**, 9011 (1988).
[15]A. W. Overhauser and A. M. de Graaf, Phys. Rev. **168**, 763 (1968).
[16]A. W. Overhauser, Phys. Rev. B **2**, 874 (1970).
[17]K. J. Duff and A. W. Overhauser, Phys. Rev. B **5**, 2779 (1972).
[18]G. F. Giuliani and A. W. Overhauser, Phys. Rev. B **22**, 3639 (1980).